Nuclear Instruments and Methods in Physics Research B 531 (2022) 100–108

Contents lists available at ScienceDirect

Nuclear Inst. and Methods in Physics Research, B

journal homepage: www.elsevier.com/locate/nimb

Evaluation of resonance parameters for neutron interactions with molybdenum

R. Mucciola [a], C. Paradela [b], G. Alaerts [b], S. Kopecky [b], C. Massimi [c], A. Moens [b], P. Schillebeeckx [b,*], R. Wynants [b]

[a] Department of Physics and Geology, University of Perugia and Sezione INFN of Perugia, Via A.Pascoli, 06123, Perugia, Italy
[b] European Commission, Joint Research Centre (JRC), Geel, Belgium
[c] Department of Physics and Astronomy, University of Bologna and Sezione INFN of Bologna, Via Irnerio 46, 40216, Bologna, Italy

ARTICLE INFO

Keywords:
Neutron resonance parameters
Transmission measurements
R-matrix analysis
Evaluation
GELINA
Molybdenum

ABSTRACT

Resonance parameters for neutron interactions with ^{92,94,95,96,97,98,100}Mo in the energy region below 5 keV were evaluated. The parameters are the result of a compilation of experimental data available in the literature together with a least squares adjustment to transmission data obtained at the time-of-flight facility GELINA. The experiments were performed at a 50 m transmission station using a ^{6}Li glass scintillator as neutron detector and metallic samples of natural Mo with a thickness of 2 mm and 5 mm. The REFIT code was used to adjust the resonance parameters, i.e. resonance energy and strength.

1. Introduction

Cross sections for neutron interactions with molybdenum are important for a broad range of scientific and technological applications ranging from nuclear astrophysics to nuclear power plant safety.

Molybdenum is found as a pollutant in pre-solar silicon carbide grains and has a crucial role in stellar nucleosynthesis in Asymptotic Giant Branch (AGB) stars [1].

In a nuclear reactor, molybdenum is produced as a fission product. It plays a role in criticality safety studies based on a burnup credit approach [2]. In addition, the use of molybdenum for the production of Accident Tolerant Fuel (ATF) is under study [3] and molybdenum is considered a promising candidate for new generation research reactors based on UMo alloys with Low Enriched Uranium (LEU) [4].

Although several experimental data sets for neutron interaction with Mo isotopes are reported in the literature, cross sections in the main evaluated nuclear data libraries are recommended with relatively large uncertainties. In this work parameters of resolved resonances for neutron interactions with ^{92,94,95,96,97,98,100}Mo were compiled from experimental data reported in the literature. Transmission measurements using metallic samples of natural molybdenum were performed at GELINA to test and adjust these parameters.

2. Experimental data reported in literature

Cross sections for neutron interactions in the resolved resonance region are parameterized by the R-Matrix formalism using individual resonance parameters [5]. For a non-fissile nuclide and for neutron interactions below the threshold of inelastic scattering, charged particle and fission reactions, a resonance is characterized by: the resonance energy (E_r), neutron width (Γ_n), radiation width (Γ_γ), total angular momentum of the final state (J) (also referred to as spin of the resonance) and neutron–nucleus orbital angular momentum (l). An accurate determination of these parameters requires a set of independent experimental observables. In most cases, transmission and radiative capture experiments are performed. From such measurements the resonance strength $K_t = g\Gamma_n$ and capture kernel $K_\gamma = g\Gamma_n\Gamma_\gamma/\Gamma$ can be derived, with the statistical factor $g = \frac{(2J+1)}{(2I+1)(2s+1)}$ defined by the spin I of the target nucleus, the spin $s = 1/2\hbar$ of the incident neutron and the total angular momentum J. In addition, the asymmetric shape of the observed transmission profiles makes it possible to identify s-wave resonances. When the width of the resonance profile is dominated by the resonance width (Doppler and resolution broadening being smaller), the resonance width can be derived from a resonance shape analysis. In some cases, a shape analysis allows the spin assignment by fitting data obtained with samples with different thicknesses. Spin and parity assignments can also be derived from γ-ray multiplicity and spectroscopic measurements.

Extensive experimental campaigns at the time-of-flight facility ORELA were carried out to determine resonance parameters for neutron interactions with the ^{92,98,100}Mo isotopes. The main interest was in

* Corresponding author.
E-mail address: peter.schillebeeckx@ec.europa.eu (P. Schillebeeckx).

https://doi.org/10.1016/j.nimb.2022.09.019
Received 9 May 2022; Received in revised form 16 September 2022; Accepted 27 September 2022
Available online 13 October 2022
0168-583X/© 2022 The Authors. Published by Elsevier B.V. This is an open access article under the CC BY license (http://creativecommons.org/licenses/by/4.0/).

a study of non-statistical effects such as valence capture. Transmission experiments using samples enriched in ^{92}Mo, ^{98}Mo and ^{100}Mo were carried out at a 80 m flight path station by Wasson et al. [6], Chrien et al. [7] and Weigmann et al. [8], respectively. Results of capture experiments for energies above 3 keV using samples enriched in ^{92,94,95,96,97,98,100}Mo were reported by Musgrove et al. [9]. The measurements were performed at a 40 m station applying the total energy detection principle using C_6F_6-scintillators. In addition, γ-ray spectroscopic measurements with a Ge-detector using samples enriched in ^{92}Mo, ^{98}Mo, and ^{100}Mo were performed at a 10 m station for spin assignments.

Experiments dedicated to spin and parity assignments of ^{94,95}Mo and ^{97}Mo are discussed by Sheets et al. [10] and Walker et al. [11], respectively. Spectra of γ-rays following neutron capture reactions were measured as a function of incident neutron energy with the DANCE detector array at the Los Alamos Neutron Science Center.

Pevzner et al. [12] investigated resonance structured cross sections for Mo isotopes by time-of-flight measurements with isotopically enriched and natural Mo samples at the neutron spectrometer in Dubna. Transmission experiments were carried out at a 110 m station and capture experiments at a 15 m station using a NaI(Tl) detector.

Capture cross section data for ^{92,94,95,96,97,98,100}Mo using isotopically enriched samples are presented by Weigmann et al. [13]. They result from measurements that were performed at a 60 m flight path station of the GELINA time-of-flight facility applying the total energy detection principle using a Moxon-Rae detector. For the even ^{92,94,96,98,100}Mo isotopes resonance parameters are reported up to about 5 keV, while for the odd ^{95,97}Mo isotopes the upper energy is 2 keV. The average ratio of the capture kernels of Weigmann et al. [13] and Musgrove et al. [9] is 1.03 with a standard deviation of 0.2.

Results of transmission experiments using natural Mo samples and samples enriched in ^{95}Mo and ^{97}Mo are discussed by Shwe and Coté [14]. The measurements were performed at a 60 m and 120 m station using the Argonne fast chopper.

Babich and Anufriev [15] reported results of transmission measurements at a 90 m flight path with a chopper for ^{98}Mo.

Transmission experiments at a 40 m and 200 m station using ^{nat}Mo samples of various thicknesses were carried out by Wynchank et al. [16] at the Columbia University synchrocyclotron.

Wang et al. [17] reports results of transmission measurements using ^{nat}Mo samples at a 10 m station of the POHANG facility.

Finally, Leinweber et al. [18] derived resonance parameters for energies below 2 keV from results of transmission and capture experiments at the RPI time-of-flight facility using ^{nat}Mo samples. The transmission measurements were performed at a 25 m station and the capture experiments at a 25 m station using a 16-segment NaI(Tl) multiplicity detector.

According to the headers in the main evaluated data libraries, there are two independent evaluated resonance parameters for Mo isotopes, i.e. those of JENDL-3.3 [19] and JENDL-4.0 [20]. The parameters of JENDL-4.0 are taken over in JEFF-3.3 [21] and those of JENDL-3.3 together with the compilation of Mughabghab [22] for ^{95}Mo are adapted in ENDF/B-VIII.0 [23]. All the recommended parameters for Mo isotopes are based on a compilation of reported parameters: i.e. resonance energy, resonance strength, and capture kernel. They do not result from a combined simultaneous or sequential resonance shape analysis of experimental transmissions or capture yields. The experimental work that was used to derive the parameters in JENDL-3.3 and JENDL-4.0 are specified in Table 1 for each isotope. The main difference between JENDL-3.3 and JENDL-4.0 is the additional transmission data of Wang et al. [17] in JENDL-4.0. At the time of writing, JENDL-5 was officially released [24]. JENDL-5 adopts the same resonance parameters as JENDL-4. The results of Leinweber et al. [18], Sheets et al. [10] and Walker et al. [11] are not used in any of the evaluated data projects.

In this paper all uncertainties are standard uncertainties quoted at a 68% confidence level and are given in standard compact notation.

Table 1
Experimental data that were used to produce the resonance parameters recommended in JENDL-3.3 [19] and JENDL-4.0 [20].

	JENDL-3.3	JENDL-4
^{92}Mo	Wasson et al. [6], Weigmann et al. [13], Musgrove et al. [9]	Wasson et al. [6], Weigmann et al. [13], Musgrove et al. [9]
^{94}Mo	Weigmann et al. [13], Musgrove et al [9],	Weigmann et al. [13], Musgrove et al. [9], Wang et al. [17]
^{95}Mo	Weigmann et al. [13], Shwe and Coté [14]	Weigmann et al. [13], Shwe and Coté [14], Wang et al. [17]
^{96}Mo	Weigmann et al. [13], Musgrove et al. [9]	Weigmann et al. [13], Musgrove et al. [9], Wang et al. [17]
^{97}Mo	Weigmann et al. [13], Shwe and Coté [14]	Weigmann et al. [13], Shwe and Coté [14], Wang et al. [17]
^{98}Mo	Weigmann et al. [13], Musgrove et al. [9], Chrien et al. [7]	Weigmann et al. [13], Musgrove et al. [9], Chrien et al. [7], Wang et al. [17], Babich et al. [15]
^{100}Mo	Weigmann et al. [13], Musgrove et al. [9], Weigmann et al. [8]	Weigmann et al. [13], Musgrove et al. [9], Weigmann et al. [8], Wang et al. [17]

3. Experiments at GELINA

Transmission experiments using natural Mo samples were performed at the time-of-flight (TOF) facility GELINA. Details about the accelerator and the neutron-producing target can be found in [25,26]. The measurements were performed at the 50 m measurement station of flight path 4, which forms an angle of 9° with the normal of the face of the moderator view in the flight path. The accelerator was operated at 400 Hz. The moderated neutron spectrum was used. A shadow bar made of Cu and Pb was placed close to the uranium target to reduce the intensity of the γ-ray flash and the fast neutron component. The samples and detector were placed in an acclimatized room to keep them at a temperature of 20 °C.

A permanent Co black resonance filter was used to continuously monitor the background at 132 eV and to account for the impact of the sample on the background [27]. Additional Na (2850 eV) and W (21.1 eV) black resonance filters were included during short cycles to estimate the background in the whole energy region. The neutron beam passing through the sample and filters was collimated to a diameter of about 4 cm and detected by a 6.35 mm thick and 101.6 mm diameter NE912 Li-glass scintillator enriched to 95% in ^{6}Li. The scintillator was connected through a boron-free quartz window to a 127 mm EMI 9823 KQB photomultiplier (PMT).

The TOF of a detected neutron was derived from the time difference between the stop signal, obtained from the anode signal of the PMT, and the start signal given at each electron burst. This time difference was processed with a multi-hit fast time coder with a 1 ns time resolution. The TOF and the pulse height of each detected event were recorded in list mode using a multi-parameter data acquisition system developed at the JRC Geel (BE). Details about the electronic set-up and data acquisition system are given in [28].

Each measurement was subdivided in different cycles. Only cycles for which the ratio between the total counts in the transmission detector and in the neutron monitor deviated by less than 1% were selected. The dead time of the detection chain t_d = 3505 (10) ns was derived from a spectrum of the time interval between successive events. The maximum dead time correction was less than 20%. In Ref. [27], it has

Table 2
Characteristics of the samples used for the transmission measurements at GELINA. The areal density is determined with an uncertainty of 0.1%.

Thickness mm	Areal density at/b	Weight g
2	1.4136 (15) × 10^{-2}	114.320 (10)
5	3.5348 (35) × 10^{-2}	251.322 (25)

been demonstrated that uncertainties due to such dead time corrections are very small and can be neglected.

The measurements were performed with ^{nat}Mo metallic samples of two different thicknesses, i.e. 2 mm and 5 mm. The 5 mm sample was obtained by stacking the 2 mm disk sample (diameter 80 mm) and six 0.5 mm thick foils (60 mm × 60 mm). The main characteristics of the samples are reported in Table 2. The areal density of the samples was derived with an uncertainty of 0.1% from a measurement of the weight and the area. The area was determined by an optical surface inspection with a microscope system from Mitutoyo [29].

The experimental transmission T_{exp} as a function of TOF was obtained from the ratio of a sample-in measurement C_{in} and a sample-out measurement C_{out}, both corrected for their background contributions B_{in} and B_{out}, respectively:

$$T_{exp} = N_t \frac{C_{in} - K B_{in}}{C_{out} - K B_{out}} \quad (1)$$

The TOF spectra C_{in} and C_{out} were corrected for losses due to the dead time in the detector and electronics chain. All spectra were normalized to the same TOF-bin width structure and neutron beam intensity. The latter was derived from the response of the BF_3 beam monitors. To avoid systematic effects due to slow variations of both the beam intensity and detector efficiency as a function of time, data were taken by alternating sample-in and sample-out measurements in cycles. Such a procedure reduces the uncertainty of the normalization to the beam intensity to less than 0.25%. This uncertainty was evaluated from the ratios of counts in the ^{6}Li transmission detector and in the beam monitors. To account for this uncertainty the factor N_t = 1.0000 (25) was introduced in Eq. (1).

The background as a function of TOF was approximated by an analytic expression applying the black resonance technique [27]. The factor K = 1.00 (3) in Eq. (1) was introduced to account for systematic effects due to the background model. Its uncertainty was derived from a statistical analysis of the difference between the observed black resonance dips and the estimated background [30]. This uncertainty is only valid for measurements with at least one fixed black resonance filters placed in the beam [27]. The time-of-flight (t) of a neutron creating a signal in the neutron detector was determined by the time difference between the stop signal (T_s) and the start signal (T_0):

$$t = (T_s - T_0) + t_0 \quad (2)$$

with t_0 a time offset which was determined by a measurement of the γ-ray flash. The flight path distance L = 47.670 (8) m, i.e. the distance between the center of the moderator viewing the flight path and the front face of the detector, was derived from results of transmission measurements using a uranium sample and the resonance energies for ^{238}U+n [31].

The analytical function used for approximating the background was a sum of a time-independent and three time-dependent components:

$$B(t) = B_0 + B_\gamma(t) + B_n(t) + B_{\tau_0}(t) \quad (3)$$

The time-independent component B_0 is related to the ambient background radiation and background contributions that lost any time correlation. The first exponential term is due to the detection of 2.2 MeV γ-rays resulting from neutron capture in hydrogen present in the moderator. The second exponential term originates predominantly from neutrons scattered inside the detector station. The third one is attributable

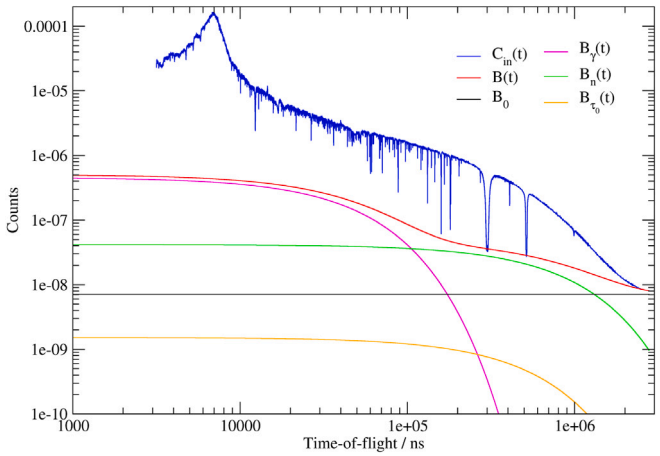

Fig. 1. Dead-time corrected TOF-spectra resulting from transmission measurements with a 2 mm thick ^{nat}Mo sample-in measurement at the 50 m station of GELINA. The total background together with the time independent and time dependent background components are shown.

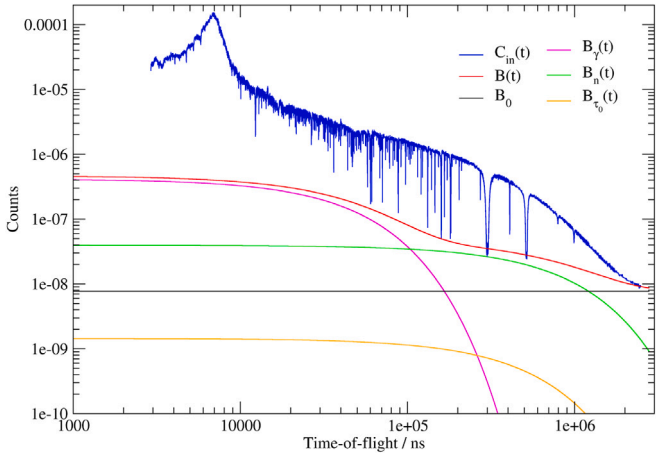

Fig. 2. Dead-time corrected TOF-spectra resulting from transmission measurements with a 5 mm thick ^{nat}Mo sample-in measurement at the 50 m station of GELINA. The total background together with the time independent and time dependent background components are shown.

to slow neutrons from previous accelerator cycles. This contribution was estimated by an extrapolation of the TOF-spectrum at the end of the cycle. The time shift τ_0 is the inverse of the accelerator frequency, i.e. τ_0 = 2.5 ms for 400 Hz. The free parameters were derived from the results of measurements with all the background filters in the beam. The amplitude of the background was adjusted to the black resonance dip at 132 eV due to the presence of the Co filter. The dead-time corrected sample-in TOF-spectra together with the background contributions resulting from the measurements with the 2 mm and 5 mm thick ^{nat}Mo samples and fixed Co black resonance filter in the beam are shown in Figs. 1 and 2 respectively.

4. Recommended resonance parameters

4.1. Resonance parameters based on a compilation of literature data

The results from the experiments discussed in Section 2 were used to construct an initial resonance parameter file for ^{92,94,95,96,97,98,100}Mo for energies below 5 keV. The resonance energies from Weigmann et al. [13] were taken as a reference. The energies from Wynchank et al. [16] and Musgrove et al. [9] were reduced by a factor 0.9995 and 0.9976, respectively.

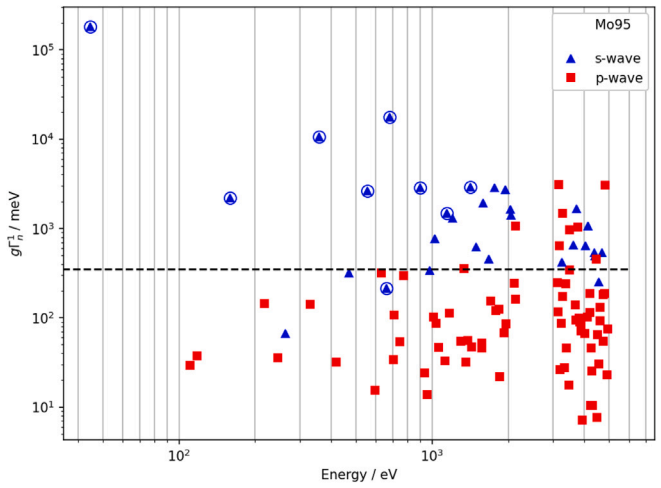

Fig. 3. Reduced neutron width of ^{95}Mo resonances as a function of neutron energy assuming all resonances are p-wave. The dashed line represents a possible separation between s-wave and p-wave resonances. The resonances for which an s-wave assignment is based on the asymmetry of the transmission profile are indicated with a circle around the triangle symbol.

The capture kernels derived by Weigmann et al. [13] were combined with those of Musgrove et al. [9] to cover an energy region up to 5 keV. For the ^{92,98,100}Mo isotopes these kernels were analyzed together with the ORELA transmission data of Refs. [6,7], and [8]. For the other isotopes, the capture data were combined with the transmission data of Wynchank et al. [16] and Leinweber et al. [18].

The parity ($l = 0$ or 1) and spin assignments for ^{92,98,100}Mo of Wasson et al. [6], Chrien et al. [7] and Weigmann et al. [8], respectively, were adopted. For ^{94,95}Mo and ^{97}Mo the assignments proposed by Sheets et al. [10] and Walker et al. [11] were implemented. Additional spin assignments for resonances with an energy below 1.5 keV were taken from Shwe and Coté [14]. The remaining assignments were taken from JENDL-4.0.

The parity assignments were verified based on the value of the reduced neutron widths of p-wave resonances. This is illustrated in Fig. 3, which plots for ^{95}Mo the reduced neutron width as a function of neutron energy supposing that all resonances are p-wave resonances. Resonances with a reduced neutron width Γ_n^1 below 350 meV can be considered as p-wave resonances. This technique has been shown to result in almost the same assignment as by applying the Bollinger and Thomas [32] approach (see e.g. Refs. [33,34]).

When both the capture kernel $K_\gamma = g\Gamma_n\Gamma_\gamma/\Gamma$ and resonance strength $K_t = g\Gamma_n$ were available, the capture width was obtained from:

$$\Gamma_\gamma = \frac{1}{g}\frac{K_t K_\gamma}{K_t - K_\gamma} \tag{4}$$

The corresponding radiation width was adopted if the value deviated by less than 50% from the average radiation width. If the deviation from the average was more than 50%, the average width was preferred. The average values were those that were used by Musgrove et al. [9] to parameterize the average capture cross sections in the unresolved resonance region by the Hauser–Feshbach formalism. They are given in Table 3. When only the capture kernel was available, the average radiation width was adopted and the neutron width was derived from:

$$\Gamma_n = \frac{\bar{\Gamma}_\gamma K_\gamma}{g\bar{\Gamma}_\gamma - K_\gamma} \tag{5}$$

The initial set of resonance parameters was verified using the results of transmission measurements performed at GELINA by comparing the experimental and theoretical transmission. For the theoretical estimate,

Table 3
Average radiation widths for s- and p-wave resonances for neutron interactions with ^{92,94,95,96,97,98,100}Mo. The values were obtained by Musgrove et al. [9].

Average radiation width, Γ_γ/meV							
	^{92}Mo	^{94}Mo	^{95}Mo	^{96}Mo	^{97}Mo	^{98}Mo	^{100}Mo
$l = 0$	160	135	150	114	130	93	85
$l = 1$	290	175	180	136	150	117	85

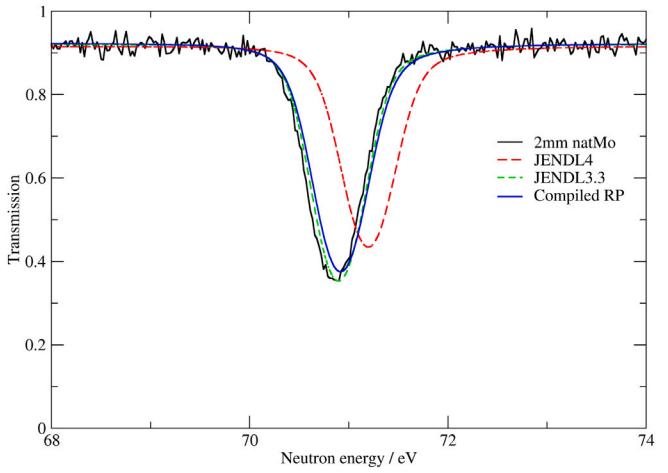

Fig. 4. Comparison between experimental and theoretical transmission for the 2 mm thick ^{nat}Mo sample in the region between 68 eV and 74 eV. The theoretical transmission is calculated using the parameters in JENDL-3.3 (green), JENDL-4 (red), and the compiled resonance parameters (blue). (For interpretation of the references to color in this figure legend, the reader is referred to the web version of this article.)

the REFIT code [35] was used. This code, which is based on the Reich-Moore approximation of the R-matrix formalism, accounts for experimental effects such as Doppler broadening, self-shielding, scattering in the sample, and the response of the TOF-spectrometer. The code also accounts for sample characteristics such as isotopic composition and impurities. The free gas model with an effective temperature of 298 K was used to describe the Doppler broadening. The time-of-flight response functions were obtained from Monte Carlo simulations. An example of such a comparison is shown in Figs. 4, 5, 6, 7 and 8. These figures clearly illustrate that based on a careful study of results reported in the literature a better quality of resonance parameters is obtained compared to the parameters that are at present recommended in the main evaluated data libraries. Fig. 4 reveals a better agreement between the experimental and theoretical transmission using the parameters recommended in JENDL-3.3 compared to those in JENDL-4. This suggests problems with the parameters reported by Wang et al. [17].

4.2. Adjustment to GELINA transmission data

The initial set of resonance parameters was improved by adjusting them in a least squares fit to the transmission data obtained at GELINA. The results of such adjustments with REFIT are shown in Figs. 6, 7 and 8. The fits were performed by adopting the spin and parity of the compiled file. Due to the presence of a permanent Co filter the parameters of the 132 eV resonance could not be adjusted. The resonance energy and neutron width of about 50% of resonances were adjusted. The adjusted parameters are listed in Table 4. The uncertainties of the adjusted parameters were derived by propagating only counting statistics uncertainties of the spectra in Eq. (1).

In the work of Weigmann et al. [13] an unresolved doublet structure around 2050 eV was observed which was assigned to ^{95}Mo. The doublet was also resolved by Wynchank et al. [16] and the two resonances were assigned to ^{95}Mo. The parameters of these resonances were adjusted

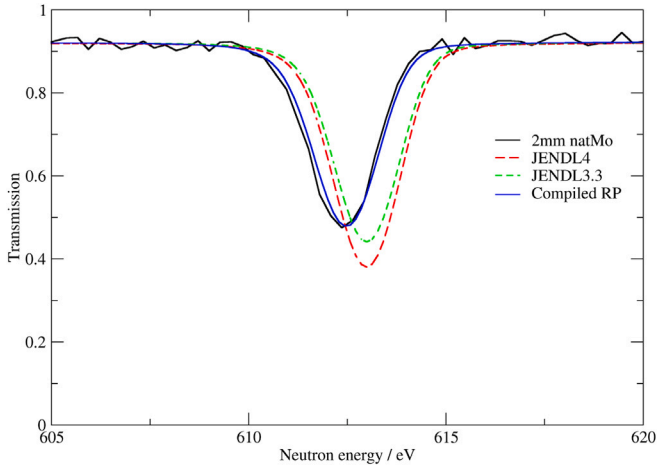

Fig. 5. Comparison between experimental and theoretical transmission for the 2 mm thick ^{nat}Mo sample in the region between 605 eV and 620 eV. The theoretical transmission is calculated using the parameters in JENDL-3.3 (green), JENDL-4 (red), and the compiled resonance parameters (blue). (For interpretation of the references to color in this figure legend, the reader is referred to the web version of this article.)

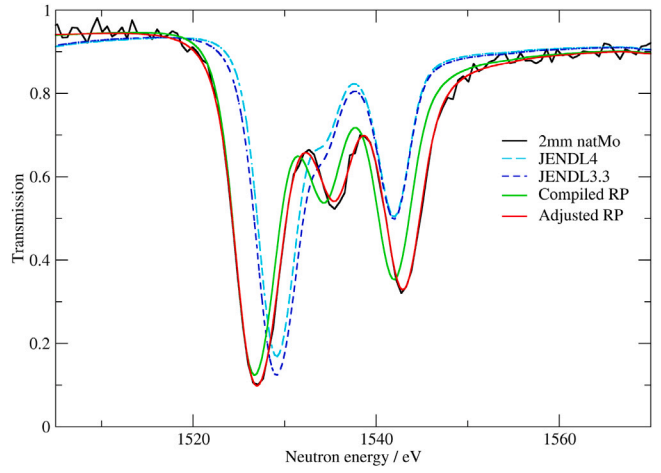

Fig. 6. Comparison between experimental and theoretical transmission for the 2 mm thick ^{nat}Mo sample in the region between 1505 eV and 1570 eV. The theoretical transmission is calculated using the parameters in JENDL-3.3 (blue), JENDL-4 (cyan), the compiled resonance parameters (green), and the adjusted resonance parameters (red). (For interpretation of the references to color in this figure legend, the reader is referred to the web version of this article.)

and the result is shown in Fig. 7. Another example of an improved description of a doublet structure using the resonance parameters obtained in this work is shown in Fig. 8.

A total of 11 unassigned resonances were observed. All these resonances were previously reported by Wynchank et al. [16]. For 5 of them, the parameters were adjusted using a radiation width of 150 meV. The results of the fit together with the values of Wynchank et al. [16] for the weaker resonances are reported in Table 5. An isotope assignment for these resonances requires additional experiments with isotopically enriched samples.

5. Conclusion

Resonance parameter files for ^{92,94,95,96,97,98,100}Mo were produced. The files are the result of a combined analysis of experimental data reported in the literature together with a resonance shape analysis of transmission data resulting from measurements at the time-of-flight facility GELINA using metallic samples of natural Mo.

Table 4
Resonance parameters, i.e. energy, resonance strength, and radiation width, for molybdenum isotopes derived in this work. The capture kernels used to derive the radiation width are given in the last column. The parameters with uncertainties between round brackets are derived from a fit to the transmission data obtained in this work. The resonance strength with uncertainties between square brackets are taken from literature data.

Isotope	Energy/eV		$J/\hbar$	$l/\hbar$	$g\Gamma_n$/meV		Γ_γ/meV		$\frac{g\Gamma_n\Gamma_\gamma}{\Gamma_n+\Gamma_\gamma}$/meV	
^{92}Mo										
	346.93	(1)	1/2[a]	0[a]	8.2	(2)	160		7.7	[5]
	1865.8	(5)	3/2[a]	1[a]	43	[10]	290		45	[3]
	2319	(1)	3/2[a]	1[a]	45	[6]	290		55	[4]
	3060.0	(1)	1/2[a]	1[a]	287	(12)	290		68	[5]
	3170.08	(6)	1/2[a]	0[a]	9147	(73)	225	(23)	220	[22]
	4285.98	(10)	3/2[a]	1[a]	1424	(36)	206	(32)	320	[38]
^{94}Mo										
	108.80		1/2	1	0.11	[3]	175		0.16	[2]
	1051.70		3/2	1	6	[2]	175		6.0	[6]
	1542.81	(1)	1/2[a]	0[a]	1647	(12)	135	(14)	125	[12]
	1660.40		3/2	1	12	[4]	175		12	[2]
	2176.78	(3)	3/2	1	964	(14)	143	(18)	220	[22]
	3159.20		3/2	1	278.20		175		155	[18]
	3571.40		3/2	1	440.32		175		195	[19]
	3595.75	(7)	1/2[a]	0[a]	2940	(49)	153	(14)	145	[13]
	4360.4	(1)	3/2	1	1509	(52)	157	(18)	260	[24]
	4616.70		1/2[a]	0[a]	514	[73]	192	(28)	140	[14]
	4927.6	(2)	1/2	1	1929	(67)	184	(17)	168	[14]
^{95}Mo										
	44.6859	(9)	3[a]	0[a]	99.4	(1)	173	(21)	50	[3]
	110.50		1[a]	1[a]	0.06	[2]	180		0.09	[2]
	118.00		2[a]	1[a]	0.09	[1]	180		0.13	[2]
	159.403	(3)	3[a]	0[a]	8.11	(5)	150		7.5	[5]
	217.93	(4)	2[a]	1[a]	0.85	(6)	180		0.97	[8]
	245.84		3[a]	1[a]	0.25	[8]	180		0.24	[3]
	263.59		2[a]	0[a]	0.5	[1]	180		0.81	[7]
	330.87	(7)	1[a]	1[a]	1.6	(1)	180		1.7	[4]
	358.499	(2)	3[a]	0[a]	131.4	(5)	167	(21)	56	[4]
	418.20		3[a]	1[a]	0.5	[2]	180		0.51	[7]
	469.70		2[a]	0[a]	5.94		180		5.5	[4]
	554.428	(7)	2[a]	0[a]	62.5	(5)	157	(30)	32	[3]
	595.67		3[a]	1[a]	0.4	[2]	180		0.4	[1]
	629.89	(5)	2[a]	1[a]	9.1	(4)	150		10.1	[6]
	661.49	(8)	3[a]	0[a]	6.7	(5)	150		8.2	[5]
	680.572	(5)	3[a]	0[a]	571	(2)	137	(11)	70	[5]
	702.77		1	1	1.2	[5]	180		1.4	[2]
	708.25		3[a]	1[a]	3.7	[5]	180		6.3	[4]
	745.46		3	1	2.0	[7]	180		3.8	[3]
	770.15	(7)	3[a]	1[a]	11.5	(6)	180		12.0	[7]
	898.85	(1)	2[a]	0[a]	140	(1)	170	(16)	47	[3]
	932.13		2[a]	1[a]	1.2	[8]	180		1.7	[3]
	956.50		4	1	0.8	[2]	180		0.8	[3]
	980.74	(7)	2[a]	0[a]	18.9	(10)	150		18	[1]
	1011.10		2	1	6	[3]	180		5.9	[5]
	1025.33	(4)	3[a]	0[a]	46	(1)	150		38	[3]
	1035.70		4	1	5	[2]	180		6.2	[5]
	1059.20		2	1	3	[1]	180		4.4	[3]
	1122.30		1	1	2.2	[8]	180		2.0	[3]
	1145.24	(2)	2[a]	0[a]	104	(2)	198	(31)	46	[4]
	1170.50		3[a]	1[a]	8	[2]	180		9.3	[7]
	1203.97	(3)	3[a]	0[a]	98	(2)	189	(31)	52	[4]
	1296.90		3	1	5	[2]	180		5.2	[5]
	1341.16	(10)	3[a]	1[a]	32	(2)	180		30	[2]
	1360.60		3	1	3	[1]	180		2.9	[4]
	1386.70		2	1	5	[2]	180		5.5	[5]
	1419.25	(2)	3[a]	0[a]	285	(3)	150	(18)	67	[6]
	1437.00		2	1	5	[2]	180		7.2	[6]
	1494.9	(1)	2[a]	0[a]	65	(4)	150		80	[7]
	1570.00		4	1	5.95		180		5.7	[4]
	1576.80		3	1	5	[2]	180		5.0	[4]
	1589.88	(3)	3[a]	0[a]	223	(4)	147	(16)	62	[5]
	1677.9	(1)	3[a]	0[a]	57	(3)	150		49	[4]
	1704.10		4	1	19.84		180		17	[1]
	1767.49	(3)	3[a]	0[a]	387	(5)	147	(15)	70	[6]
	1788.00		4	1	17	[8]	180		24	[2]

(*continued on next page*)

Table 4 (*continued*).

Isotope	Energy/eV		$J/\hbar$	$l/\hbar$	$g\Gamma_n$/meV		Γ_γ/meV		$\frac{g\Gamma_n\Gamma_\gamma}{\Gamma_n+\Gamma_\gamma}$/meV	
	1841.70		3	1	18	[5]	180		16	[1]
	1853.30		3	1	3.19		180		3.1	[4]
	1925.10		3	1	10	[1]	180		15	[1]
	1950.61	(3)	2[a]	0[a]	424	(7)	145	(13)	53	[4]
	1961.30		3	1	14	[8]	180		12.0	[9]
	2044.72	(5)	2	0	275	(6)	150			
	2050.44	(6)	2[a]	0[a]	239	(6)	150			
	2116.1	(6)	1	1	43	[14]	189	(75)	23	[2]
	2131.46	(6)	3	1	191	(6)	181	(21)	68	[5]
	2140.90		1	1	29	[9]	114	(38)	14	[1]
	3125	(2)	4	1	79.41		180		50	[6]
	3146.43		2	1	37.50		180		25	[3]
	3166.9	(2)	4	1	1009	(66)	151	(20)	102	[12]
	3184.35		1	1	208.12		180		37	[5]
	3209.28		3	1	8.66		180		8	[2]
	3235.22		4	1	29.19		180		24	[3]
	3250.7	(6)	3	0	141.04		150		54	[6]
	3276.12		2	1	58.93		180		33	[5]
	3279.6	(4)	1	1	504	(74)	150	(23)	35	[5]
	3340.96		4	1	9.64		180		9	[2]
	3366.2	(5)	1	1	86	(11)	141	(25)	25	[3]
	3392.84		1	1	16.36		180		12	[2]
	3463.67		2	1	6.52		180		6	[2]
	3488.50		1	1	130	[6]	149	(27)	29	[4]
	3501.2	(2)	1	1	364	(16)	94	(14)	22	[3]
	3623.1	(2)	3	0	260	(15)	142	(21)	63	[7]
	3673.16		1	1	56.25		180		25	[3]
	3694.50		1	1	38	[38]	180		16	[3]
	3723.7	(1)	2	0	685	(21)	132	(17)	51	[6]
	3756	(1)	4	1	434.53		180		103	[12]
	3809.83		2	1	42.19		180		27	[4]
	3830.40		4	1	39	[39]	180		58	[7]
	3866.40		4	1	31	[20]	180		37	[5]
	3879.40		1	1	39	[31]	180		21	[3]
	3921.57		1	1	3.21		180		3	[1]
	4009.35		4	1	30.68		180		25	[3]
	4030.8	(2)	2	0	300	(20)	141	(21)	49	[6]
	4105.12		4	1	49.09		180		36	[5]
	4135.8	(2)	2	0	515	(24)	133	(18)	50	[6]
	4191.91		4	1	56.84		180		40	[5]
	4213.20		1	1	94	[41]	180		15	[2]
	4227.83		4	1	5.19		180		5	[1]
	4260.75		3	1	23.20		180		19	[3]
	4281.70		1	1	12.86		180		10	[2]
	4306.64		2	1	5.36		180		5	[1]
	4383.5	(4)	3	0	282	(24)	154	(24)	68	[8]
	4394.7	(4)	3	0	263	(25)	139	(21)	62	[7]
	4449.30		4	1	244.69		180		87	[11]
	4478.23		3	1	4.16		180		4	[1]
	4518.13		4	1	35.33		180		28	[4]
	4555.00		4	1	17	[17]	180		24	[3]
	4565.02		3	0	141.04		150		54	[7]
	4601.93		2	1	52.84		180		31	[4]
	4612.90		1	1	74.12		180		28	[4]
	4700.2	(4)	3	0	312	(26)	109	(18)	53	[7]
	4737.00		4	1	108	[43]	180		77	[9]
	4757.55		3	1	32.81		180		25	[4]
	4793.47		2	1	112.50		180		45	[6]
	4837.2	(1)	4	1	1851	(53)	165	(21)	116	[14]
	4921.16		2	1	14.29		180		12	[2]
	4948.10		4	1	47.25		180		35	[5]
^{96}Mo										
	113.35	(2)	1/2	1	0.45	(2)	136		0.45	[4]
	131.40		1/2[a]	0[a]	259.8	[6]	88	(7)	66	[4]
	419.04	(3)	1/2	1	5.8	(2)	136		5.8	[4]
	968.41		1/2	1	2.4	[9]	136		2.7	[4]
	1267.00		1/2	1	1.1	[5]	136		2.2	[3]
	1497.78	(8)	1/2	1	79	(4)	136		9.4	[7]
	2088.9	(1)	1/2	1	69	(4)	136		7	[1]
	2363.14	(2)	1/2[a]	0[a]	4122	(23)	164	(16)	158	[15]
	2484.40		1/2	1	60	[24]	136		27	[2]
	2778.0	(2)	1/2	1	119	(8)	73	(11)	45	[4]

(*continued on next page*)

Table 4 (*continued*).

Isotope	Energy/eV		$J/\hbar$	$l/\hbar$	$g\Gamma_n$/meV		Γ_γ/meV		$\frac{g\Gamma_n\Gamma_\gamma}{\Gamma_n+\Gamma_\gamma}$/meV	
	3284.35	(10)	1/2[a]	0[a]	15294	(86)	184	(28)	182	[27]
	3571.65	(4)	1/2	0	7252	(41)	103	(8)	102	[8]
	3756	(6)	3/2	1	184.69		136		110	[9]
	4320.3	(2)	1/2	0	500	(26)	88	(10)	75	[7]
	4412.10		3/2	1	127.91		136		87	[8]
	4560.00		1/2	1	16	[16]	136		40	[4]
	4941.90		1/2	1	20.75		136		18	[4]
^{97}Mo										
	70.8660	(10)	2[a]	0[a]	8.06	(3)	127	(55)	7.0	[4]
	79.55		3	1[a]	0.04	[1]	150		0.06	[2]
	109.58		1[a]	1[a]	0.09	[2]	150		0.11	[4]
	126.89		3	1	0.13	[2]	150		0.10	[4]
	136.32		3[a]	1	0.34	[4]	150		0.57	[5]
	209.98		1[a]	1[a]	0.38	[8]	150		0.54	[5]
	227.58		3[a]	1	1.0	[1]	150		1.26	[9]
	233.33		1	1	0.35	[6]	150		0.33	[5]
	247.91		3	1	0.8	[2]	150		0.78	[7]
	267.93	(1)	3[a]	0[a]	8.7	(1)	130		8.0	[5]
	285.907	(3)	2[a]	0[a]	46.2	(3)	110	(16)	23	[2]
	311.85	(3)	3	0[a]	5.0	(2)	130		5.1	[4]
	321.12		3	1	0.8	[2]	150		0.9	[1]
	352.51	(6)	4[a]	1[a]	4.4	(3)	150		4.2	[5]
	380.94	(6)	2[a]	1	3.1	(3)	150		2.9	[2]
	397.063	(6)	3[a]	0[a]	42.9	(4)	119	(20)	26	[2]
	457.30		3[a]	1	0.9	[3]	150		0.8	[1]
	505.21	(2)	2[a]	0[a]	32.6	(6)	142	(27)	21	[1]
	528.45		2	1	0.7	[4]	150		21.0	[1]
	533.81		3[a]	1	2.0	[6]	150		2.2	[2]
	548.25		1	1	2.5	[4]	150		2.2	[2]
	557.974	(4)	3[a]	0[a]	291	(2)	135	(11)	62	[4]
	564.06		1	1	1.3	[5]	150		1.3	[6]
	568.00		4	1	2.9	[6]	150		3.2	[4]
	571.97		1	1	2.9	[8]	150		2.7	[4]
	578.52		4	1	0.8	[4]	150		0.8	[1]
	653.16		2[a]	1	1.5	[6]	150		1.3	[2]
	675.873	(7)	3	0[a]	192	(2)	130		78	[7]
	694.68		4[a]	1[a]	5	[1]	150		5.8	[4]
	700.74		3	1	4	[2]	150		4.4	[3]
	786.37	(1)	3[a]	0[a]	177	(2)	152	(15)	59	[4]
	809.20		4	1	1.7	[8]	150		1.9	[3]
	862.70	(7)	2[a]	0	24	(1)	130		20	[1]
	905.68		1	1	5	[2]	150		4.7	[4]
	975.14		2[a]	1	5	[2]	150		6.5	[5]
	1008.25	(7)	2[a]	0	37	(2)	145	(28)	23	[2]
	1108.30	(2)	3	0	215	(3)	87	(8)	41	[3]
	1133.40		2	1	9	[3]	150		21	[1]
	1177.4	(1)	2[a]	0	34	(2)	130		27	[2]
	1194.20		4	1	4.69		150		4.5	[4]
	1250.04	(1)	3[a]	0[a]	807	(6)	121	(10)	65	[5]
	1271.7	(2)	2[a]	0	24	(3)	130		20	[1]
	1293.50		2[a]	1	12	[5]	150		16	[1]
	1317.60		4	1	27	[8]	150		22	[2]
	1333.50		3	1	20	[6]	150		20	[1]
	1365.7	(2)	2[a]	1	25	(3)	150		24	[2]
	1375.40		3	1	8	[3]	150		5.3	[7]
	1398.00		2	1	6	[3]	150		6.5	[7]
	1425.0	(1)	3[a]	0	45	(3)	130		32	[2]
	1453.10		1	1	10.99		150		8	[1]
	1485.00		3	1	6	[2]	150		5.5	[7]
	1535.25	(2)	3[a]	0[a]	598	(9)	104	(8)	55	[4]
	1554.20		2	1	3	[1]	150		2.8	[5]
	1596.9	(2)	3[a]	1	59	(4)	200	(55)	39	[3]
	1628.40		3	1	3	[2]	130		6.6	[7]
	1699.00		4	1	64	[10]	91	(19)	33	[2]
	1713.24	(6)	3	0	205	(6)	129	(13)	55	[4]
	1740.70		2	1	19.91		150		15	[1]
	1795.00		3	1	22	[7]	150		20	[2]
	1835.90		2	1	7	[3]	150		6.3	[8]
	1865.00		4	1	9	[4]	150			
	1870.90		1	1	10	[5]	150			
	1903.80		3	1	38.84		150		27	[2]
	1931.50		2	1	21	[8]	130		36	[3]
	1942.9	(3)	3	0	64	(7)	161	(41)	38	[3]

(*continued on next page*)

Table 4 (*continued*).

Isotope	Energy/eV		$J/\hbar$	$l/\hbar$	$g\Gamma_n$/meV		Γ_γ/meV		$\frac{g\Gamma_n\Gamma_\gamma}{\Gamma_n+\Gamma_\gamma}$/meV	
	3055.65		1	1	53.23		150		22	[3]
	3070.61		4	1	14.70		150		13	[2]
	3076.60		3	1	70.36		150		39	[5]
	3114.1	(4)	3	0	133	(16)	140		60	[7]
	3125	(2)	4	1	153.95		150		65	[8]
	3146.43		4	1	8.61		150		8	[1]
	3172.37		2	1	27.30		150		19	[2]
	3184.5	(2)	2	0	688	(42)	99	(13)	39	[5]
	3207.70		2	0	148	[53]	130		15	[2]
	3217.70		1	1	30	[30]	150		14	[2]
	3244.20		3	1	27.63		150		21	[3]
	3259.16		1	1	59.48		150		23	[3]
	3281.11		3	0	99.31		130		43	[5]
	3311.03		3	1	19.58		150		16	[2]
	3349.94		1	1	7.14		150		6	[1]
	3363.91		3	1	24.27		150		19	[2]
	3374.88		3	0	89.26		130		41	[5]
	3389.5	(3)	2	0	266	(21)	120	(17)	42	[5]
	3420.77		1	1	31.10		150		17	[2]
	3468.66		2	1	14.85		150		12	[2]
	3484.62		1	1	15.57		150		11	[2]
	3495.59		1	1	66.67		150		24	[3]
	3528.51		2	0	91.32		130		34	[5]
	3549.46		3	1	24.27		150		19	[3]
	3583.38		4	1	4.15		150		4	[1]
	3601.34		4	1	8.61		150		8	[1]
	3615.30		3	1	12.58		150		11	[1]
	3642.50		1	1	32	[32]	150		3	[1]
	3649.00		2	0	316	[63]	130		13	[2]
	3670.20		1	1	63	[63]	150		9	[1]
	3702.09		3	1	12.58		150		11	[2]
	3710.07		2	1	57.69		150		30	[4]
	3718.05		3	1	35.00		150		25	[4]
	3783.90		1	1	22.34		150		14	[2]
	3827.79		2	1	9.17		150		8	[1]
	3839.76		2	1	9.17		150		8	[1]
	3843.40		1	1	32	[32]	150		17	[2]
	3854.73		2	1	18.04		150		14	[2]
	3872.68		3	0	146.77		130		50	[6]
	3912.59		2	1	69.92		150		33	[4]
	3980.42		4	1	75.00		150		45	[5]
^{98}Mo										
	12.076	(2)	3/2	1[a]	0.0673	(7)	117		0.058	[4]
	401.70	(3)	3/2	1[a]	2.9	(1)	117		3.2	[2]
	429.306	(3)	1/2	1[a]	66.9	(3)	147	(41)	46	[4]
	467.535	(3)	1/2[a]	0[a]	799	(1)	95	(10)	85	[8]
	612.382	(6)	1/2	1[a]	62.0	(4)	164	(40)	45	[3]
	817.983	(7)	3/2	1[a]	129.1	(10)	112	(26)	82	[7]
	1122.85	(8)	3/2	1[a]	16.4	(8)	117		19	[1]
	1526.910	(9)	1/2[a]	0[a]	1574	(7)	71	(7)	68	[6]
	1922.20		3/2	1[a]	12	[5]	117		20	[2]
	2024.5	(4)	1/2	1[a]	17	(3)	117		2.5	[2]
	2166.7	(1)	1/2	1[a]	60	(3)	117		73	[6]
	2462.53	(10)	1/2	1[a]	123	(4)	100	(17)	55	[5]
	2548.89	(2)	1/2[a]	0[a]	1143	(11)	69	(7)	65	[6]
	2601.4	(2)	3/2	1[a]	68	(5)	117		41	[4]
	2945.60		1/2	1[a]	21	[6]	117		39	[4]
	3260.80		1/2	1[a]	18	[14]	117		37	[4]
	3297.24	(7)	1/2[a]	0[a]	1728	(60)	83	(9)	79	[8]
	3797.4	(1)	3/2	1[a]	424	(13)	104	(15)	140	[13]
	4014.43	(10)	3/2	1[a]	510	(15)	77	(9)	118	[11]
	4478.7	(1)	1/2[a]	0[a]	566	(19)	82	(9)	72	[7]
	4569.79	(9)	3/2	1[a]	1025	(25)	92	(10)	156	[14]
	4847.9	(1)	3/2	1[a]	855	(33)	105	(12)	168	[15]
^{100}Mo										
	97.31	(2)	3/2[a]	1[a]	0.48	(2)	85		0.36	[3]
	364.017	(2)	1/2[a]	0[a]	627	(1)	70	(7)	63	[6]
	507.05	(9)	1/2	1[a]	5.1	(5)	85		4.2	[3]
	535.81		1/2	1[a]	5.80		85		4.0	[3]
	785.68		1/2	1[a]	6.70		85		5.4	[4]
	1069.45	(2)	1/2[a]	1[a]	123	(2)	85		80	[7]
	1260.88	(4)	3/2	1[a]	99	(3)	91	(25)	64	[6]

(*continued on next page*)

Table 4 (*continued*).

Isotope	Energy/eV		$J/\hbar$	$l/\hbar$	$g\Gamma_n$/meV		Γ_γ/meV		$\frac{g\Gamma_n\Gamma_\gamma}{\Gamma_n+\Gamma_\gamma}$/meV	
	1404.47	(5)	1/2[a]	0[a]	112	(3)	47	(6)	33	[3]
	1697.23	(4)	3/2	1[a]	325	(6)	72	(9)	100	[9]
	1767.8	(4)	1/2	1[a]	21	[2]	85		17	[2]
	1937.81	(3)	1/2[a]	0[a]	1008	(14)	56	(6)	53	[5]
	2061.70		1/2	1	6	[2]	85		6.0	[7]
	2420.89	(6)	3/2	1[a]	516	(12)	56	(6)	92	[8]
	2630.9	(1)	1/2[a]	0[a]	360	(13)	66	(7)	56	[5]
	2663.00		1/2	1	12	[4]	85		11	[1]
	2951.60		3/2	1	42	[6]	85		39	[4]
	3006.64	(5)	1/2[a]	0[a]	1840	(26)	50	(5)	49	[5]
	3071.5	(1)	1/2[a]	1[a]	377	(17)	51	(5)	45	[4]
	3260.80		3/2	1	137	[7]	64	(13)	66	[7]
	3536.00		3/2	1	52	[5]	85		42	[5]
	3547.00		1/2	1	99	[6]	76	(16)	43	[5]
	3601.70		3/2	1	123	[8]	57	(12)	59	[6]
	4151.00		3/2	1	18.89		85		17	[2]
	4510.6	(3)	1/2	0	638	(40)	75	(8)	67	[6]
	4543.00		3/2	1	134.21		85		75	[7]
	4727.50		1/2	1	200	[107]	58	(11)	45	[4]

[a]The parity and spin assignments that were derived from experimental data.

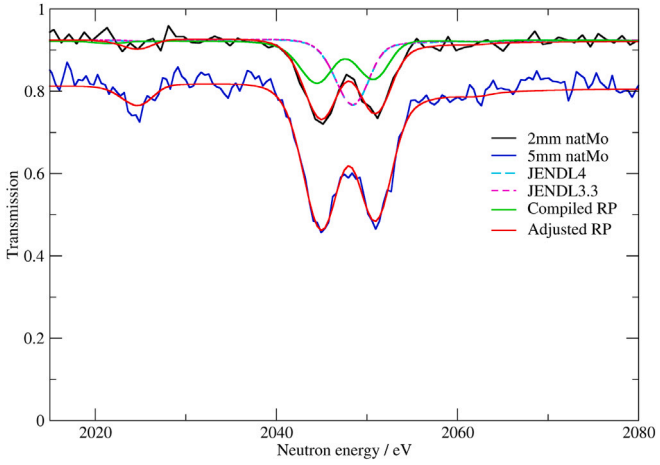

Fig. 7. Comparison between experimental and theoretical transmission for the 2 mm and 5 mm thick ^{nat}Mo sample in the region between 2015 eV and 2080 eV. The theoretical transmission is calculated using the parameters in JENDL-3.3 (magenta), JENDL-4 (cyan), the compiled resonance parameters (green), and the adjusted resonance parameters (red). For the 5 mm sample, only the theoretical curve with the adjusted parameters is shown. (For interpretation of the references to color in this figure legend, the reader is referred to the web version of this article.)

Table 5
Resonance energy and observed strength ($ag\Gamma_n$) for 11 unassigned resonances. The resonance strength can be derived using the isotopic abundance a once an isotope assignment is made. The parameters with uncertainties between round brackets are derived from a fit to the transmission data obtained in this work. The resonance strengths with uncertainties between square brackets are taken from Wynchank et al. [16].

Energy/eV		$ag\Gamma_n$/meV	
2298.05		7	[2]
2371.9	(1)	29	(2)
2437.6	(2)	17	(1)
2578.40	(9)	39	(1)
2613.0	(3)	12	(1)
2695.65		7	[3]
2728.68		6	[3]
2758.62		8	[3]
2841.78		8	[5]
3039.5	(1)	59	(2)
4127.00		6	[6]

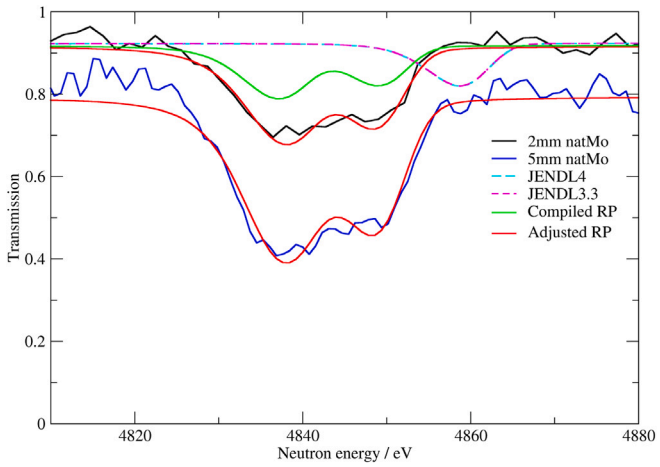

Fig. 8. Comparison between experimental and theoretical transmission for the 2 mm and 5 mm thick ^{nat}Mo sample in the region between 4810 eV and 4880 eV. The theoretical transmission is calculated using the parameters in JENDL-3.3 (magenta), JENDL-4 (cyan), the compiled resonance parameters (green), and the adjusted resonance parameters (red). For the 5 mm sample, only the theoretical curve with the adjusted parameters is shown. (For interpretation of the references to color in this figure legend, the reader is referred to the web version of this article.)

The results in this paper reveal that the parameters recommended in the evaluated data libraries do not always reflect the quality of the data that is available in the literature and that improved parameters can already be derived from an adjustment to transmission data obtained with natural samples. For an additional improvement capture and transmission measurements with isotopically enriched samples are required. An effort is ongoing within the EU project SANDA to perform capture and transmission experiments using samples enriched in ^{94,95,96}Mo [36].

CRediT authorship contribution statement

R. Mucciola: Formal analysis, Data curation, Investigation, Writing – original draft. **C. Paradela:** Methodology, Supervision, Validation, Writing – review & editing. **G. Alaerts:** Methodology, Writing – review & editing. **S. Kopecky:** Supervision, Validation, Writing – review & editing. **C. Massimi:** Validation, Writing – review & editing. **A. Moens:** Methodology, Supervision, Validation, Writing – review & editing. **P. Schillebeeckx:** Methodology, Supervision, Validation, Writing – review & editing. **R. Wynants:** Methodology, Writing – review & editing.

Declaration of competing interest

The authors declare the following financial interests/personal relationships which may be considered as potential competing interests: Riccardo Mucciola reports financial support was provided by Euratom Research and Training Programme.

Data availability

Data will be made available on request.

Acknowledgment

This work was supported by the EUFRAT open-access project of the JRC Geel, Belgium. This project has received funding from the Euratom research and training programme 2014–2018 under grant agreement No 847594 (ARIEL).

References

[1] N. Liu, T. Stephan, S. Cristallo, R. Gallino, P. Boehnke, L.R. Nittler, C.M.O. Alexander, A.M. Davis, R. Trappitsch, M.J. Pellin, I. Dillmann, Astrophys. J. 881 (2019) 28.
[2] I. Gauld, G. Ilas, G. Radulescu, Technical Report NUREG/CR-7012, US Nuclear Regulatory Commission, 2011.
[3] B. Cheng, Y. Kim, P. Chou, Nucl. Eng. Technol. (ISSN: 1738-5733) 48 (2016) 16–25.
[4] X. Iltis, H. Palancher, J. Allenou, F. Vanni, B. Stepnik, A. Leenaers, S.V.D. Berghe, D. Keiser, I. Glagolenko, EPJ Nucl. Sci. Technol. 4 (2018) 49.
[5] F.H. Fröhner, Evaluation and Analysis of Nuclear Resonance Data, JEFF Report 18, NEA/OCDC, 2000.
[6] O.A. Wasson, G.G. Slaughter, Phys. Rev. C 8 (1973) 297–314.
[7] R.E. Chrien, G.W. Cole, G.G. Slaughter, J.A. Harvey, Phys. Rev. C 13 (1976) 578–594.
[8] H. Weigmann, S. Raman, J.A. Harvey, R.L. Macklin, G.G. Slaughter, Phys. Rev. C 20 (1979) 115–127.
[9] A. De L. Musgrove, B. Allen, J. Boldeman, R. Macklin, Nuclear Phys. A 270 (1976) 108–140.
[10] S.A. Sheets, U. Agvaanluvsan, J. Becker, F. Bečvář, T.A. Bredeweg, R.C. Haight, M. Krtička, M. Jandel, G.E. Mitchell, J.M. O'Donnell, W.E. Parker, R. Reifarth, R.S. Rundberg, E. Sharapov, I. Tomandl, J.L. Ullmann, D.J. Vieira, J.M. Wouters, J.B. Wilhelmy, C.Y. Wu, Phys. Rev. C 76 (2007) 064317.
[11] C.L. Walker, M. Krtička, B. Baramsai, F. Bečvář, T.A. Bredeweg, A. Chyzh, R.C. Haight, M. Jandel, J. Kroll, G.E. Mitchell, J.M. O'Donnell, R.S. Rundberg, J.L. Ullmann, S. Valenta, J.B. Wilhelmy, Phys. Rev. C 92 (2015) 014324.
[12] M.I. Pevzner, J. Exp. Theor. Phys. 17 (1963) 803.
[13] H. Weigmann, G. Rohr, J. Winter, Proceedings of the Third Conference on Neutron Cross Sections and Technology, Conf-710301, Vol. 2, National Technical Information Center, Springfield, Virginia, 1971, p. 749.
[14] H. Shwe, R.E. Coté, Phys. Rev. 179 (1969) 1148–1153.
[15] S.I. Babich, V.A. Anufriev, Atom. Energiya 67 (1989) 140.
[16] S. Wynchank, J.B. Garg, W.W. Havens, J. Rainwater, Phys. Rev. 166 (1968) 1234–1254.
[17] T.F. Wang, A.K.M.M.H. Meaze, M.U. Khandaker, M.S. Rahman, G.N. Kim, L.P. Zhu, H.H. Xia, Z.Y. Zhou, Y.D. Oh, H. Kang, M.H. Cho, I.S. Ko, W. Namkung, Nucl. Instrum. Methods Phys. Res. B 266 (2008) 561–569.
[18] G. Leinweber, D.P. Barry, J.A. Burke, N.J. Drindak, Y. Danon, R.C. Block, N.C. Francis, B.E. Moretti, Nucl. Sci. Eng. 164 (2010) 287–303.
[19] K. Shibata, T. Kawano, T. Nakagawa, O. Iwamoto, J. Katakura, T. Fukahori, S. Chiba, A. Hasegawa, T.M. andH. Matsunobu, T. Ohsawa, Y. Nakajima, T. Yoshida, A. Zukeran, M. Kawai, M. Baba, M. Ishikawa, T. Asami, T. Watanabe, Y. Watanabe, M. Igashira, N. Yamamuro, H. Kitazawa, N. Yamano, H. Takano, J. Nucl. Sci. Technol. 39 (2002) 1125–1136.
[20] K. Shibata, O. Iwamoto, T. Nakagawa, N. Iwamoto, A. Ichihara, S. Kunieda, S. Chiba, K. Furutaka, N. Otuka, T. Ohsawa, T. Murata, H. Matsunobu, A. Zukeran, S. Kamada, J. Katakura, J. Nucl. Sci. Technol. 48 (2011) 1–30.
[21] A.J.M. Plompen, O. Cabellos, C.D.S. Jean, M. Fleming, A. Algora, M. Angelone, P. Archier, E. Bauge, O. Bersillon, A. Blokhin, F. Cantargi, A. Chebboubi, C. Diez, H. Duarte, E. Dupont, J. Dyrda, B. Erasmus, L. Fiorito, U. Fischer, D. Flammini, D. Foligno, M.R. Gilbert, J.R. Granada, W. Haeck, F.-J. Hambsch, P. Helgesson, S. Hilaire, I. Hill, M. Hursin, R. Ichou, R. Jacqmin, B. Jansky, C. Jouanne, M.A. Kellett, D.H. Kim, H.I. Kim, I. Kodeli, A.J. Koning, A.Y. Konobeyev, S. Kopecky, B. Kos, A. Krása, L.C. Leal, N. Leclaire, P. Leconte, Y.O. Lee, H. Leeb, O. Litaize, M. Majerle, J.I.M. Damián, F. Michel-Sendis, R.W. Mills, B. Morillon, G. Noguère, M. Pecchia, S. Pelloni, P. Pereslavtsev, R.J. Perry, D. Rochman, A. Röhrmoser, P. Romain, P. Romojaro, D. Roubtsov, P. Sauvan, P. Schillebeeckx, K.H. Schmidt, O. Serot, S. Simakov, I. Sirakov, H. Sjöstrand, A. Stankovskiy, J.C. Sublet, P. Tamagno, A. Trkov, S. van der Marck, F. Álvarez-Velarde, R. Villari, T.C. Ware, K. Yokoyama, G. Žerovnik, Eur. Phys. J. A 56 (2020) 181.
[22] S. Mughabghab, Atlas of Neutron Resonances, Elsevier.
[23] D. Brown, M. Chadwick, R. Capote, A. Kahler, A. Trkov, M. Herman, A. Sonzogni, Y. Danon, A. Carlson, M. Dunn, D. Smith, G. Hale, G. Arbanas, R. Arcilla, C. Bates, B. Beck, B. Becker, F. Brown, R. Casperson, J. Conlin, D. Cullen, M.-A. Descalle, R. Firestone, T. Gaines, K. Guber, A. Hawari, J. Holmes, T. Johnson, T. Kawano, B. Kiedrowski, A. Koning, S. Kopecky, L. Leal, J. Lestone, C. Lubitz, J. Márquez Damián, C. Mattoon, E. McCutchan, S. Mughabghab, P. Navratil, D. Neudecker, G. Nobre, G. Noguere, M. Paris, M. Pigni, A. Plompen, B. Pritychenko, V. Pronyaev, D. Roubtsov, D. Rochman, P. Romano, P. Schillebeeckx, S. Simakov, M. Sin, I. Sirakov, B. Sleaford, V. Sobes, E. Soukhovitskii, I. Stetcu, P. Talou, I. Thompson, S. van der Marck, L. Welser-Sherrill, D. Wiarda, M. White, J. Wormald, R. Wright, M. Zerkle, G. Žerovnik, Y. Zhu, Nucl. Data Sheets 148 (2018) 1–142.
[24] O. Iwamoto, N. Iwamoto, K. Shibata, A. Ichihara, S. Kunieda, F. Minato, S. Nakayama, EPJ Web Conf. 239 (2020) 09002.
[25] W. Mondelaers, P. Schillebeeckx, Notiziario Neutroni Luce Sci. 11 (2006).
[26] D. Tronc, J. Salomé, K. Böckhoff, Nucl. Instrum. Methods A 228 (1985) 217–227.
[27] P. Schillebeeckx, B. Becker, Y. Danon, K. Guber, H. Harada, J. Heyse, A. Junghans, S. Kopecky, C. Massimi, M. Moxon, N. Otuka, I. Sirakov, K. Volev, Nucl. Data Sheets 113 (2012) 3054–3100.

[28] C. Paradela Dobarro, J. Drohe, J. Heyse, S. Kopecky, S. Moscati, L. Salamon, P. Schillebeeckx, D. Vendelbo, R. Wynants, Electronic Setup for Time-Of-Flight Cross Section Measurements at GELINA, Publications Office of the European Union, Luxembourg, ISBN: 978-92-76-43927-1, 2021, http://dx.doi.org/10.2760/477469.
[29] https://www.mitutoyo.co.jp/eng/ (08/09/2022).
[30] I. Sirakov, B. Backer, R. Capote, E. Dupont, S. Kopecky, C. Massimi, P. Schillebeeckx, Eur. Phys. J. A 49 (2013) 144.
[31] H. Derrien, L.C. Leal, N.M. Larson, A. Courcelle, ORNL/TM-2005/241, Oak Ridge, 2005.
[32] L.M. Bollinger, G.E. Thomas, Phys. Rev. 171 (1968) 1293–1297.
[33] K. Volev, A. Borella, S. Kopecky, C. Lampoudis, C. Massimi, A. Moens, M. Moxon, P. Schillebeeckx, P. Siegler, I. Sirakov, A. Trkov, R. Wynants, Nucl. Instrum. Methods Phys. Res. B (ISSN: 0168-583X) 300 (2013) 11–29.
[34] H.I. Kim, C. Paradela, I. Sirakov, B. Becker, R. Capote, F. Gunsing, G.N. Kim, S. Kopecky, C. Lampoudis, Y.. Lee, R. Massarczyk, A. Moens, M. Moxon, V. Pronyaev, P. Schillebeeckx, R. Wynants, Eur. Phys. J. A 52 (2016) 170.
[35] M.C. Moxon, J.B. Brisland, AEA-InTec-0630, AEA Technology, 1991.
[36] https://cordis.europa.eu/project/id/847552 (08/09/2022).